Influence of fabrication disorder on the optical properties of coupled-cavity photonic crystal waveguides

D. P. Fussell, S. Hughes, and M. M. Dignam

Department of Physics, Queen's University, Kingston, Ontario, Canada, K7L 3N6

Employing a tight-binding formalism and perturbation theory, we theoretically demonstrate how weak fabrication disorder due to surface roughness dramatically reduces the band-edge performance of coupled-cavity waveguides in semiconductor photonic crystal slabs. We find that surface roughness largely affects the band-edge performance through the introduction of random variations in the individual cavity frequencies, Ω_0, rather than through variations in the tight-binding coupling coefficients, κ. Using model roughness parameters comparable to state-of-the-art structures, the standard deviation of Ω_0 is estimated to be $\sigma_{\omega_0} \gtrsim 1 \times 10^{-4} \; \Omega_0$. High-index-contrast fabrication imperfections are found to broaden the photon density of states at the band edge with a characteristic linewidth of $\gamma_e \approx \sigma_{\omega_0}^{4/3}/(2 \; \Omega_0 \kappa)^{1/3}$. This implies a *minimal* band-edge group velocity of around $v_g \sim c/120$, consistent with experiments. For applications toward modified spontaneous emission, we show that the characteristic linewidth γ_e is, unfortunately, a factor of 5 greater than the largest band-edge coupling rate for which strong photon quantum dot band-edge interactions can occur. Although large Purcell factors can still be achieved in the presence of disorder, an embedded semiconductor quantum dot then couples to a lossy (disorder-induced) propagation mode, which may limit the potential applications in coherent quantum optics.

I. INTRODUCTION

Light propagates in coupled-cavity waveguides (CCWs) via the evanescent coupling of localized cavity modes.[1,2] CCWs are currently under active interest within the optics community since, in principle, they can support small group velocities, either across their bandwidth when the separation between the cavities is large or at their well-defined photonic band edges. Slow light in CCWs has several significant applications including buffering and storing optical pulses[3,4] and enhancing nonlinear optical interactions such as second-harmonic generation.[5] In addition, the small group velocity at the band edge of CCWs potentially produces strong interactions with atoms and quantum dots (QDs); thus, CCWs could be used for single-photon sources due to the large Purcell factor and high directionality[6,7] or alternatively could serve as a test bed for the novel physics of band-edge quantum optics.[8]

Photonic crystal (PhC) slabs (PhCSs) are an appealing platform for CCWs as it is relatively straightforward to engineer large arrangements of coupled cavities. The experimental performance of early CCWs in PhCS (Refs. [9–11]) was limited by the low Q (quality factor) of the PhCS cavities available at the time. Cavities have since been designed to minimize out-of-plane loss producing ultrahigh Q's above 1×10^6.[12,13] Waveguiding in CCWs based on these cavities has also recently been demonstrated in experiments.[13,14] A key feature of *intrinsic loss* in CCWs in PhCSs is that it is not solely determined by the Q's of the constituent cavities.[15,16] Rather, the interference of the out-of-plane radiation from the cavities can cause the Q's of the CCW modes to depend on the Bloch vector. It is typically found, though, that the Q's of the CCW modes remain within an order of magnitude of the Q's of the individual cavities.

From a theory and modeling perspective, an additional advantage of CCWs is that the well-known tight-binding approach can be exploited,[1] facilitating a way to include the effects of fabrication imperfections that result in *extrinsic loss*. In the tight-binding approximation, fabrication imperfections cause variations in the cavity frequencies, which are termed as *diagonal disorder*, and in the coupling coefficients, it is termed as *off-diagonal* disorder. Both types of disorder are well researched in condensed-matter physics, e.g., by Economou *et al.*,[17,18] but less so in photonics. Steinberg *et al.*[19] considered diagonal disorder due to random variations in the size of the dielectric cylinders of PhCs and demonstrated that transmission bands are maintained so long as the standard deviation of the cavity frequencies is smaller than the CCW bandwidth. Mookherjea and Oh[20] heuristically considered off-diagonal disorder due to surface roughness in general CCWs; by calculating the group velocity via the density of states (DOS), they showed that minimal roughness of a few nanometer limited the slowing factor—the ratio of the band-center group velocity to the band-edge group velocity—to less than 10. This result is broadly consistent with experiment.[21,22]

In this paper, we critically examine the role of disorder-induced surface roughness on the band-edge performance of CCWs in PhCSs. Surface roughness can be characterized from scanning electron microscopy (SEM) images,[23] although a quantitative characterization requires many Fourier components,[23] making the precise analysis of its effects difficult. A more standard and reliable approach is to model the roughness as random variations in the dielectric function about the perfect structure with a standard deviation of σ_e and correlation length of l_c.[24] Hughes *et al.*[25] used this approach to successfully describe extrinsic loss in line-defect waveguides in PhCSs and accurately reconciled theory with experiment.[26] Here, we adopt a similar approach to model the effect of surface roughness on diagonal and off-diagonal disorders in CCWs in PhCSs. We show how the broadening of the band-edge DOS by the disorder can be quantified. We
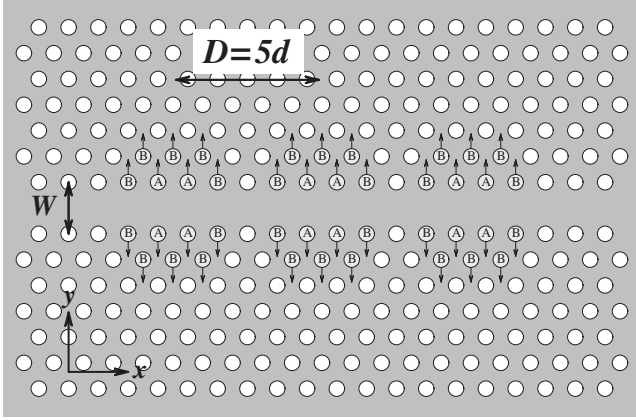
FIG. 1. Schematic of the CCW composed of PhCS cavities formed by the local width modulation of a line-defect waveguide. The PhCS period is d, the CCW period is $D=5d$, and the width of the line defect is $W=\sqrt{3}d$.

then examine the effect of the DOS broadening on the group velocity and band-edge interactions with QDs. We find that even state-of-the-art fabrication disorder will likely limit the propagation speed in CCWs to no less than $c/200$. We also find that it will be very difficult to get strong coupling at the band edge due to disorder-induced softening of the band-edge DOS. On the other hand, we find that reasonably large Purcell factors should be possible even when disorder is present, thus, opening the possibility that these structures could be exploited to produce highly directional single-photon sources.

The paper is organized as follows. In Sec. II, we present our tight-binding formalism for calculating the modes and the DOS for a coupled-mode system such as a CCW. This formalism involves calculating the individual cavity modes and mode frequencies as well as the tight-binding coupling coefficients. In Sec. III, we examine the statistical effects of surface roughness disorder on the individual cavity-mode frequencies and the coupling coefficients. In Sec. IV, we present the effects of the surface roughness on the DOS in a CCW. In Sec. V, we discuss the consequences of surface roughness on slow-light propagation and band-edge quantum optics in CCWs. We present our conclusions in Sec. VI.

II. TIGHT-BINDING FORMALISM

We begin by presenting the tight-binding formalism for CCWs. The CCW consists of a set of coupled defect cavities that are arranged in the x direction with a period D. An example CCW (to be discussed in detail later) is shown in Fig. 1. We consider both infinite and finite CCWs composed of N cavities. To obtain the dispersion relation for a CCW, we employ the tight-binding approach. In this approach, the νth CCW complex mode is expanded in terms of the N individual cavity modes, $\widetilde{\mathbf{M}}_q(\mathbf{r}-\mathbf{R}_q)$, as $\widetilde{\mathbf{M}}_\nu^{CCW}(\mathbf{r}) = \Sigma_{q=1}^N v_{q\nu}\widetilde{\mathbf{M}}_q(\mathbf{r}-\mathbf{R}_q)$, where $\mathbf{R}_q=qD\hat{\mathbf{x}}$ is the position of the qth cavity and $\hat{\mathbf{x}}$ is a unit vector along x. The (leaky) mode of the qth cavity has a (complex) frequency $\widetilde{\Omega}_q$ and is normalized according to the condition
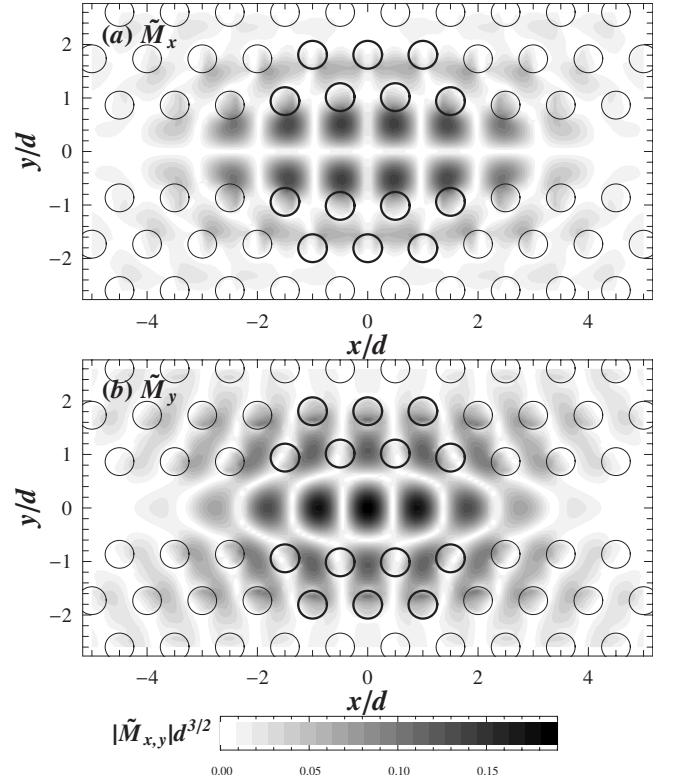

FIG. 2. Cavity mode (x/y field) of the PhCS cavity formed by the local width modulation of a line-defect waveguide.

$$\int_{V_c} d^3\mathbf{r}\,\epsilon_q(\mathbf{r})|\widetilde{\mathbf{M}}_q(\mathbf{r}-\mathbf{R}_q)|^2 = 1, \tag{1}$$

where V_c is the computed field domain [e.g., from finite-difference time domain (FDTD)] and $\epsilon_q(\mathbf{r})$ is the (real) dielectric constant of the structure with a single cavity centered at $\mathbf{r}=\mathbf{R}_q$. The frequency is complex due to the finite lifetime of the mode arising from *intrinsic* out-of-plane leakage. The CCW modes are then the eigensolutions to

$$(\mathbf{I}+\mathbf{K})^{-1}\mathbf{\Omega}\,\mathbf{v} = \mathbf{\Lambda}\mathbf{v}, \tag{2}$$

where $\mathbf{K}=[\kappa_{pq}]$ with $\kappa_{pq}=\int d\mathbf{r}\,\delta\epsilon_q(\mathbf{r})\widetilde{\mathbf{M}}_p^*(\mathbf{r}-\mathbf{R}_p)\cdot\widetilde{\mathbf{M}}_q(\mathbf{r}-\mathbf{R}_q)$ and $\delta\epsilon_q(\mathbf{r})\equiv\epsilon(\mathbf{r})-\epsilon_q(\mathbf{r})$, where $\epsilon(\mathbf{r})$ is the dielectric function of the structure with the full set of cavities in the CCW. The other matrices are defined by: $\mathbf{v}\equiv[v_{\nu q}]$, $\mathbf{\Omega}=\text{Diagonal}\{\widetilde{\Omega}_q^2\}$, and $\mathbf{\Lambda}=\text{Diagonal}\{\widetilde{\omega}(k_\nu)^2\}$, where $\widetilde{\omega}(k_\nu)$ is the frequency of the CCW mode with mode index k_ν.

For the CCW of Fig. 1, in the absence of surface roughening, all of the cavities are identical and differ only by their position; thus $\widetilde{\mathbf{M}}_q(\mathbf{r})=\widetilde{\mathbf{M}}_0(\mathbf{r})$ and $\widetilde{\Omega}_q=\widetilde{\Omega}_0$. In Fig. 2 we plot the x and y components of the single-cavity mode field $\widetilde{\mathbf{M}}_0(\mathbf{r})$. The chosen CCW has a period of $D=5d$, which makes the cavity coupling sufficiently weak to employ the nearest-neighbor tight-binding (NNTB) approximation. In this approximation,

$$\kappa_{pq} = \kappa \equiv \int d\mathbf{r} \, \delta\epsilon_0(\mathbf{r}) \tilde{\mathbf{M}}_0^*(\mathbf{r} + D\hat{x}) \cdot \tilde{\mathbf{M}}_0(\mathbf{r}) \tag{3}$$

if $p = q \pm 1$ and is zero otherwise. In the nearest-neighbor approximation, the dispersion relation that follows from Eq. (2) is[27]

$$\tilde{\omega}(k_\nu) = \tilde{\Omega}_0[1 - \kappa \cos(k_\nu D)], \tag{4}$$

where $k_\nu = \nu\pi/[(N+1)D]$, where $\nu = 1 \dots N$. In an infinite CCW with periodic boundary conditions, the same dispersion relation holds,[1] but $k_\nu \to k$ with $-\pi/D \leq k \leq \pi/D$ and the CCW mode expansion coefficients become $v_{qk} = e^{iqkD}$.

The analytic form of Eq. (4) results in simple expressions for the local density of states (LDOS). We obtain the LDOS from the electric-field Green tensor.[28] For coupling to a QD with transition dipole $\boldsymbol{\mu} = \mu\hat{\mathbf{d}}$, the *projected* LDOS is obtained from the *total* Green tensor, $\tilde{\mathbf{G}}$, using

$$\text{LDOS}(\omega;\mathbf{r}) = -2\omega/\pi c^2 \, \text{Im}\{\hat{\mathbf{d}} \cdot \tilde{\mathbf{G}}(\omega;\mathbf{r},\mathbf{r}) \cdot \hat{\mathbf{d}}^*\}. \tag{5}$$

The total Green tensor is the solution to

$$\nabla \times \nabla \times \tilde{\mathbf{G}}(\omega;\mathbf{r},\mathbf{r}') - \frac{\omega^2}{c^2}\epsilon(\mathbf{r})\tilde{\mathbf{G}}(\omega;\mathbf{r},\mathbf{r}') = -\mathbf{I}\delta(\mathbf{r} - \mathbf{r}'). \tag{6}$$

However, we typically calculate the *transverse* Green tensor, $\tilde{\mathbf{G}}^T$, which is the solution to

$$\nabla \times \nabla \times \tilde{\mathbf{G}}^T(\omega;\mathbf{r},\mathbf{r}') - \frac{\omega^2}{c^2}\epsilon(\mathbf{r})\tilde{\mathbf{G}}^T(\omega;\mathbf{r},\mathbf{r}') = -\mathbf{I}\delta^T(\mathbf{r} - \mathbf{r}'), \tag{7}$$

where $\delta^T(\mathbf{r} - \mathbf{r}')$ is the transverse Dirac delta function.[29] For media with a real dielectric constant, $\epsilon(\mathbf{r})$, it follows that[30]

$$\tilde{\mathbf{G}}(\omega;\mathbf{r},\mathbf{r}') = \tilde{\mathbf{G}}^T(\omega;\mathbf{r},\mathbf{r}') - \frac{\mathbf{I}\delta^T(\mathbf{r} - \mathbf{r}')}{(\omega/c)^2\epsilon(\mathbf{r})} + \frac{\mathbf{I}\delta(\mathbf{r} - \mathbf{r}')}{(\omega/c)^2\epsilon(\mathbf{r})}. \tag{8}$$

Thus, we can also express the LDOS in terms of the transverse Green tensor,

$$\text{LDOS}(\omega;\mathbf{r}) = -2\omega/\pi c^2 \, \text{Im}\{\hat{\mathbf{d}} \cdot \tilde{\mathbf{G}}^T(\omega;\mathbf{r},\mathbf{r}) \cdot \hat{\mathbf{d}}^*\}. \tag{9}$$

The transverse Green tensor has a well-known expansion over the true transverse modes of the structure.[28] However, the true modes form a continuum and extend over all space and are thus an impractical basis for most problems. To address this, we recently showed that in resonant structures such as a CCW composed of high-Q cavities, an accurate expression for the transverse Green tensor can be obtained by projecting it onto the resonant modes (the CCW modes in our case).[31] In the nearest-neighbor approximation, the projection yields the *tight-binding Green tensor* given by[8]

$$\tilde{\mathbf{G}}_{\text{TB}}^T(\omega;\mathbf{r},\mathbf{r}') = \frac{c^2}{2\omega}\sum_\nu \sum_{p,q=1}^N \tilde{\mathbf{M}}_p(\mathbf{r})\frac{v_{p\nu}u_{\nu q}}{\omega - \tilde{\omega}(k_\nu)}\tilde{\mathbf{M}}_q^*(\mathbf{r}'), \tag{10}$$

where $\mathbf{u} \equiv \mathbf{v}^{-1} = [u_{\nu p}]$. The LDOS is then obtained by using Eq. (10) for the Green tensor in Eq. (9), yielding

$$\text{LDOS}(\omega;\mathbf{r})$$
$$= -\frac{1}{\pi}\sum_\nu \sum_{p,q=1}^N \text{Im}\left\{\hat{\mathbf{d}} \cdot \tilde{\mathbf{M}}_p(\mathbf{r})\frac{v_{p\nu}u_{\nu q}}{\omega - \tilde{\omega}(k_\nu)}\tilde{\mathbf{M}}_q^*(\mathbf{r}) \cdot \hat{\mathbf{d}}^*\right\}. \tag{11}$$

As the $\tilde{\mathbf{M}}_q$ has a very small spatial overlap, if a QD is at $\mathbf{r}$ near the center of the q_0th cavity, then $|\tilde{\mathbf{M}}_{q_0}(\mathbf{r})| \gg |\tilde{\mathbf{M}}_p(\mathbf{r})|$ for $p \neq q_0$ and the LDOS simplifies to

$$\text{LDOS}(\omega;\mathbf{r}) = -\frac{1}{\pi\epsilon(\mathbf{r})V(\mathbf{r})}\sum_{\nu=1}^N \text{Im}\left\{\frac{v_{q_0\nu}u_{\nu q_0}}{\omega - \tilde{\omega}(k_\nu)}\right\}, \tag{12}$$

where

$$V^{-1}(\mathbf{r}) \equiv \epsilon(\mathbf{r})|\tilde{\mathbf{M}}_{q_0}(\mathbf{r}) \cdot \hat{\mathbf{d}}|^2 \tag{13}$$

is the spatially dependent mode volume. If $\mathbf{r}$ is at a mode maximum and $\hat{\mathbf{d}}$ is parallel to $\tilde{\mathbf{M}}_{q_0}(\mathbf{r})$, then $V(\mathbf{r}) = V_{\text{eff}}$, where V_{eff} is the "usual" effective mode volume commonly used, e.g., in calculations of the Purcell factor or enhanced spontaneous emission factor.[32] For the cavity mode computed in Fig. 2, the effective mode volume is $V_{\text{eff}} \sim 0.175 \ \mu m^3$.

As we can see from Eq. (12), the LDOS is in fact just the DOS, $\rho(\omega)$, divided by $\epsilon(\mathbf{r})V(\mathbf{r})$,

$$\text{LDOS}(\omega;\mathbf{r}) = \frac{\rho(\omega)}{\epsilon(\mathbf{r})V(\mathbf{r})}. \tag{14}$$

This can be verified by the fact that the integral of $\rho(\omega)$ over ω gives the number of quasimodes in the system. This is useful since, while it is the LDOS that primarily determines the spontaneous emission dynamics of a QD, we can analyze the dynamics by studying the much simpler quantity $\rho(\omega)$. This point has been exploited before for regular planar photonic crystal waveguides.[6,33]

In a finite CCW, we obtain

$$\rho(\omega) = -\frac{1}{\pi}\sum_{\nu=1}^N \text{Im}\left\{\frac{v_{q_0\nu}u_{\nu q_0}}{\omega - \tilde{\omega}(k_\nu)}\right\}, \tag{15}$$

while in an infinite CCW $u_{\nu q_0} = v_{q_0\nu}^\dagger = e^{-iqkD}$ and we can do the sum explicitly to obtain simply

$$\rho(\omega) = -\frac{1}{\pi}\text{Im}\left\{\frac{1}{\sqrt{(\omega - \tilde{\omega}_u)(\omega - \tilde{\omega}_l)}}\right\}. \tag{16}$$

The structure that we model is the CCW first introduced by Kuramochi *et al.*[13] shown in Fig. 1. We choose this structure due to its low intrinsic loss and because it has been experimentally investigated. This planar structure includes a high-Q PhCS cavity formed by the local width modulation of a line-defect waveguide.[26] The PhCS consists of a hexagonal array of cylindrical air voids of radius $a = 0.26d$, where $d = 420$ nm is the period in a silicon (or high-index) dielectric slab of refractive index $n = 3.46$ and height $h = 0.5d$. The cavities are formed by moving the air-voids labeled "A" in Fig. 1 away from the waveguide by $0.15d$ and the air-voids labeled B by $0.075d$. The cavity mode is calculated using the full three-dimensional (3D) FDTD method. As the cavity mode is
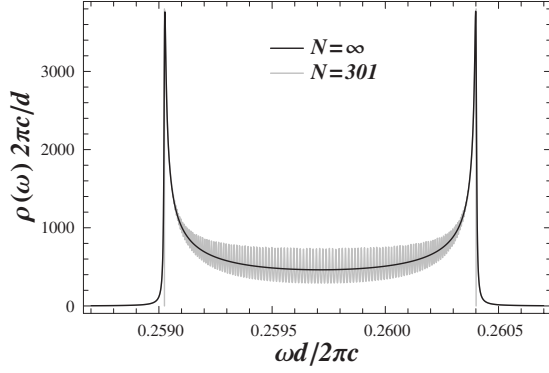
FIG. 3. DOS in periodic ($N=\infty$) and finite ($N=301$) CCWs.

leaky, it is characterized by a *complex* frequency, $\widetilde{\Omega}_0 = \Omega_0 - i\gamma_0 = (0.260 - i3.37 \times 10^{-6})2\pi c/d$, resulting in a quality factor of $Q_0 = 38\,600$. Using Eq. (3), the tight-binding coupling coefficient is found to be $\kappa = 0.002\,65$. Note that while κ is in principle complex,[16] for this structure the imaginary part is sufficiently small that it can be neglected.

In Fig. 3, we plot the DOS of the Kuramochi *et al.* system for frequencies that span the CCW band for both $N=301$ [Eq. (15)] and ∞ [Eq. (16)]. The midband oscillations of the $N=301$ DOS are due to the finite-size Fabry-Perot effects. At the band edges, the DOS exhibits the expected inverse square-root behavior. In a lossless CCW ($\gamma_0 = 0$) with $N=\infty$, the band-edge DOS would be singular. When loss is included ($\gamma_0 > 0$), the band-edge DOS is finite and the square-root line shape about the band edge broadens. However, in our CCW, the DOS and corresponding LDOS at the band edges are large enough for QD-photon interactions to enter the strong-coupling regime.[8] It is also strong enough to result in the slowing of light by several orders of magnitude. The key questions that we address in the remainder of this paper are: What are the effects of surface roughening on the DOS, and how do the changes in the DOS affect QD-photon interactions and slow-light modes? In Sec. III we consider the effects of surface roughness on the individual cavity-mode frequencies, $\widetilde{\Omega}_0$, and on the tight-binding coupling coefficients, κ.

III. INFLUENCE OF SURFACE ROUGHNESS ON MODE FREQUENCIES AND COUPLING COEFFICIENTS

The true dielectric function of a fabricated CCW, $\epsilon_t(\mathbf{r})$, includes small random variations due to the fabrication process. As a consequence, $\epsilon_t(\mathbf{r})$ differs from the dielectric function of the ideal structure, $\epsilon(\mathbf{r})$, by the function $\Delta\epsilon(\mathbf{r}) \equiv \epsilon_t(\mathbf{r}) - \epsilon(\mathbf{r})$. In the tight-binding model of Eq. (2), $\Delta\epsilon(\mathbf{r})$ results both in variations in the diagonal elements $\widetilde{\Omega}_0$ (consequently called diagonal disorder) and variations in the off-diagonal elements κ (consequently called off-diagonal disorder). Both of these forms of disorder have been well researched in solid-state physics[17] primarily to understand the effects of disorder on conductivity. Here, we first examine the influence of diagonal disorder on the DOS and near the end of this section consider the effects of off-diagonal disorder.

We account for diagonal disorder by employing first-order perturbation theory to determine the variations in the $\widetilde{\Omega}_0$. This is appropriate for the weak fabrication disorder that we anticipate to be present in a state-of-the-art PhCS. We define the disorder perturbation on the ideal dielectric structure with a single cavity at $\mathbf{r}=0$ as $\Delta\epsilon_0(\mathbf{r}) \equiv \epsilon_{0t}(\mathbf{r}) - \epsilon_0(\mathbf{r})$, where $\epsilon_{0t}(\mathbf{r})$ is the true dielectric function for the system with a single cavity and disorder and $\epsilon_0(\mathbf{r})$ is the dielectric function of the same system without disorder. Ignoring the effects of local-field corrections and boundary conditions of the field components across the perturbed hole interface (which we briefly discuss below), the first-order shift in the mode frequency can be calculated using[19]

$$\delta\widetilde{\omega}_0 \simeq -\frac{\widetilde{\Omega}_0}{2}\int_{V_c} d^3\mathbf{r}\,\Delta\epsilon_0(\mathbf{r})|\widetilde{\mathbf{M}}_0(\mathbf{r})|^2, \qquad (17)$$

where, as usual with perturbation theory, the unperturbed $\widetilde{\Omega}_0$ and $\widetilde{\mathbf{M}}_0(\mathbf{r})$ are used. Because $\widetilde{\Omega}_0$ is complex and the integral in Eq. (17) is real, we see that the ratio of the real to imaginary parts of the perturbed frequency, $\widetilde{\Omega}_0 + \delta\widetilde{\omega}_0$, is the same as for the unperturbed frequency. Thus, to the first order in the perturbation, the Q of the cavity mode is unchanged. Therefore, in what follows we will largely concern ourselves with the real part of the frequency shift, which we denote by $\delta\omega_0$.

In the structure that we are modeling (see Fig. 1), the cavity modes are 3D TE-type modes. Therefore, they can have some electric-field components that are perpendicular to the cylinder boundaries and are thus discontinuous across the cylinder boundaries. If Eq. (17) is to be an accurate method for calculating the frequency shift, the mode field of the perturbed structure should be similar to that of the unperturbed structure in the vicinity of the cylinder boundaries. We would expect this to be the case if the component of the field component perpendicular to the cylinder boundary is relatively small relative to the tangential component for the unperturbed structure. From Fig. 2 we see that the tangential component appears to be generally larger than the perpendicular component (as desired). However, in addition, for high-index contrast structures there can be local-field corrections that cause an asymmetry in the disorder function with respect to the interface.[34] Although in principle we should properly include local-field effects and carefully account for parallel and perpendicular components across the perturbed dielectric interface, other works have shown that when applied to a disorder problem such as ours, these corrections largely average out[35] or primarily result in an overall system shift of the single-cavity resonance.[36] Thus, we do not include such effects here.

To estimate the accuracy of Eq. (17) for our structure, we have varied the radii of the air voids in a "selected" random fashion (shown in bold) in Fig. 2 by several nanometers, which is comparable to the scale of the surface roughness that we will examine shortly. We then calculated $\delta\omega_0$ numerically using a FDTD simulation and compared with $\delta\omega_0$ that is found using Eq. (17). We note that the small positional shifts result in $\Delta\epsilon(\mathbf{r})$ being nonzero only near the air-void
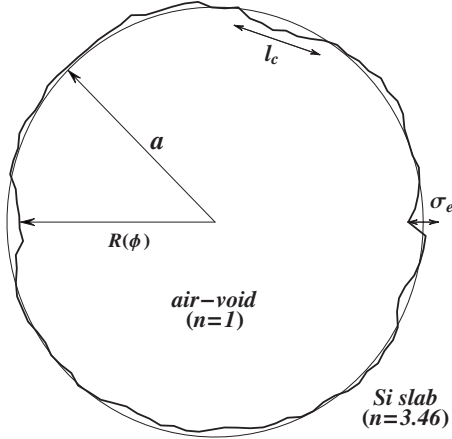
FIG. 4. Surface roughness on the circumference of an air void. The radius of the air void becomes a function of angle $R(\phi)$. The surface roughness is characterized by a standard deviation of σ_e and a correlation length of l_c.

boundaries, and so we only need to carry out the integrations around the surface of the air voids. To calculate Eq. (17), $\widetilde{\mathbf{M}}_0(\mathbf{r})$ is approximated using an interpolation function to obtain field points on the interface of the air voids through the discrete mesh of field points generated by the FDTD simulation. We find that the frequency shift given by our first-order calculation agrees with the "numerically exact" (FDTD) result to within 10%. This degree of accuracy is more than sufficient for the present work as a 10% error is more than the uncertainty in the roughness parameters. The inclusion of the local-field corrections will be dealt with in future work, however, such corrections will not affect significantly the physics and predictions which we highlight here. We further emphasize that similar approaches presented elsewhere,[25] on the subject of disorder-induced waveguide loss (more details given below), have been very successful in their predictive capabilities and have explained a number of recent experiments (e.g., Kuramochi et al.[26]).

We model fabrication disorder by adopting the approach of Hughes et al.[25] Their approach is similar to the technique of the well-known Payne and Lacey approach for ridge waveguides[24] but specialized to periodic media such as PhCSs. In PhCSs, the dominant fabrication imperfection is surface roughness in the form of vertical striations in the sidewalls of the air voids. The effect on the dielectric function of a single air void is demonstrated schematically in Fig. 4. The striations cause random variations in $\epsilon_{0t}(\mathbf{r})$, which are characterized by the deviation $\Delta \epsilon_0(\mathbf{r})$, such that $\epsilon_{0t}(\mathbf{r}) = \epsilon_0(\mathbf{r}) + \Delta \epsilon_0(\mathbf{r})$. Now, by construction, $\Delta \epsilon_0(\mathbf{r})$ is such that the ensemble average of $\Delta \epsilon_0(\mathbf{r})$ is zero,

$$\langle \Delta \epsilon_0(\mathbf{r}) \rangle = 0, \qquad (18)$$

where $\langle \cdot \rangle$ denotes the average over an ensemble of structures. Thus, if we take the average shift of an ensemble of our structures, we find that

$$\langle \delta \omega_0 \rangle = -\frac{\Omega_0}{2} \int_{V_c} d^3 \mathbf{r} \langle \Delta \epsilon_0(\mathbf{r}) \rangle |\widetilde{\mathbf{M}}_0(\mathbf{r})|^2 \qquad (19)$$

$$= 0. \qquad (20)$$

Note that while there may be a frequency shift due to roughness in an individual structure, the average shift over many structures will be zero—at least within the limitations of our model. To determine the statistics of the frequency shifts of such an ensemble, we calculate the variance in the frequency shift of the ensemble. This is given by

$$\langle [\delta \omega_0]^2 \rangle \simeq \frac{\Omega_0^2}{4} \int_{V_c} \int_{V_c} d^3 \mathbf{r} \, d^3 \mathbf{r}' |\widetilde{\mathbf{M}}_0(\mathbf{r})|^2 |\widetilde{\mathbf{M}}_0(\mathbf{r}')|^2$$
$$\times \langle \Delta \epsilon_0(\mathbf{r}) \Delta \epsilon_0(\mathbf{r}') \rangle. \qquad (21)$$

The standard deviation of the frequency shifts in the ensemble due to the perturbation is then given by $\sigma_{\Omega_0} = \sqrt{\langle [\delta \omega_0]^2 \rangle}$.

The roughness function is incorporated in $\Delta \epsilon_0(\mathbf{r})$ as follows. In a PhCS containing multiple air voids, the center position of the lth air void is denoted by $\boldsymbol{\rho}_l$, where $\boldsymbol{\rho} = (\rho, \phi)$ is the in-plane coordinate. For an air void at $\boldsymbol{\rho}_l$, the roughness function is given by $\Delta R[\widetilde{\phi}(\boldsymbol{\rho}, \boldsymbol{\rho}_l)]$, where $\widetilde{\phi}(\boldsymbol{\rho}, \boldsymbol{\rho}_l) = \arctan[(\rho \sin \phi - \rho_l \sin \phi_l)/(\rho \cos \phi - \rho_l \cos \phi_l)]$ is the translated coordinate. For an air void at the origin, $\Delta R[\widetilde{\phi}(\boldsymbol{\rho}, \boldsymbol{\rho}_l)] = \Delta R(\phi)$ as above. By expanding the exact dielectric profile, which contains a Heaviside step function at each hole interface, to first order, then

$$\Delta \epsilon_0(\mathbf{r}) \simeq (\epsilon_2 - \epsilon_1) H(h/2 - |z|) \sum_{l=1}^{N_c} R[\widetilde{\phi}(\boldsymbol{\rho}, \boldsymbol{\rho}_l)] \delta(a - |\boldsymbol{\rho} - \boldsymbol{\rho}_l|),$$
$$(22)$$

where $\epsilon_1(\epsilon_2)$ is the dielectric constant outside (inside) the air voids, $H(z)$ is the Heaviside step function, and N_c is the number of air voids of the cavity; the slab thickness is h, and the slab center coincides with $z = 0$. As the roughness is due to vertical striations in the air-void walls, the air-void radius is a random function of angle, $R(\phi)$, but is independent of z. The difference from ideal is then described by the *roughness function* $\Delta R(\phi) = R(\phi) - a$ for each hole (in a shifted-coordinate scheme). The roughness function has an ensemble average of $\langle \Delta R(\phi) \rangle = 0$ and an ensemble root-mean square of $\sigma_e = [\langle \Delta R^2(\phi) \rangle]^{1/2}$. The roughness function is also correlated as a function of ϕ, which is described using a model exponential autocorrelation function,

$$C(\phi - \phi') = \langle \Delta R(\phi) \Delta R(\phi') \rangle, \qquad (23)$$

$$= \sigma_e^2 e^{-a \Theta(\phi, \phi')/l_c}, \qquad (24)$$

where

$$\Theta(\phi, \phi') = \begin{cases} |\phi - \phi'| & \text{if } 0 \le |\phi - \phi'| < \pi, \\ 2\pi - |\phi - \phi'| & \text{if } \pi \le |\phi - \phi'| < 2\pi, \end{cases}$$
$$(25)$$

is the *angular displacement* between two points on the cir-

cumference of the air void and l_c is the in-plane correlation length. As can be seen in Fig. 4, σ_e describes the characteristic amplitude of the roughness about the circumference, while l_c describes the characteristic *correlation* length of the deviations along the circumference. For high-quality fabricated silicon PhCSs, $\sigma_e \gtrsim 3$ nm and $l_c \approx 40$ nm.[26] In our PhCS ($d = 420$ nm), the corresponding normalized values are $\sigma_e \gtrsim 0.007d$ and $l_c \approx 0.1d$.

We now return to the calculation of the standard deviation in the frequency shift for an ensemble of structures. Inserting Eq. (22) into Eq. (21), and then using Eq. (24) to take the ensemble average, we obtain the standard deviation

$$
\sigma_{\Omega_0} \simeq \sigma_e(\epsilon_2 - \epsilon_1)\frac{\Omega_0}{2}\Bigg\{ \sum_{l=1}^{N_c} \int_{-h/2}^{h/2}\int_{-h/2}^{h/2} dz\,dz' \int_0^{2\pi}\int_0^{2\pi} d\phi\,d\phi'
$$

$$
\times e^{-a\Theta(\phi,\phi')/l_c}|\widetilde{\mathbf{M}}_0
$$

$$
\times [x_l + a\cos(\phi), y_l + a\sin(\phi), z]|^2|\widetilde{\mathbf{M}}_0
$$

$$
\times [x_l + a\cos(\phi'), y_l + a\sin(\phi'), z']|^2 \Bigg\}^{1/2}, \qquad (26)
$$

where (x_l, y_l) is the in-plane coordinate of the lth air void.

Having examined the effect of surface roughness on the distribution of individual cavity-mode frequencies (diagonal

disorder), we now treat the effect of the surface roughness on the tight-binding coupling coefficient (off-diagonal disorder). To do this, we simply add $\Delta\epsilon(\mathbf{r})$ in our definition of κ given in Eq. (3). This yields a change in the coupling coefficient by an amount

$$
\delta\kappa \simeq \int_{V_c} d^3\mathbf{r}\, \delta\epsilon_{0t}(\mathbf{r})\widetilde{\mathbf{M}}_0(\mathbf{r}+D\hat{\mathbf{x}}) \cdot \widetilde{\mathbf{M}}_0^*(\mathbf{r}), \qquad (27)
$$

where $\delta\epsilon_{0t}(\mathbf{r}) \equiv \Delta\epsilon(\mathbf{r}) - \Delta\epsilon_0(\mathbf{r})$, and $\Delta\epsilon(\mathbf{r})$ is the difference between the exact and the perturbed dielectric functions for the full coupled-cavity waveguides (CCW) structure. The statistical properties of $\delta\kappa$ are again determined by the statistical properties of $R(\phi)$. As $\langle R(\phi)\rangle = 0$, it follows immediately that the mean perturbation is zero, i.e., $\langle\delta\kappa\rangle = 0$. However, the standard deviation of the perturbation is not zero but is given by $\sigma_\kappa = [\langle\delta\kappa^2\rangle]^{1/2}$, where

$$
\delta\kappa^2 \simeq \int_{V_c}\int_{V_c} d^3\mathbf{r}\,d^3\mathbf{r}'\, \delta\epsilon_{0t}(\mathbf{r})\widetilde{\mathbf{M}}_0(\mathbf{r}+D\hat{\mathbf{x}}) \cdot \widetilde{\mathbf{M}}_0^*(\mathbf{r})\delta\epsilon_{0t}
$$

$$
\times(\mathbf{r}')\widetilde{\mathbf{M}}_0(\mathbf{r}'+D\hat{\mathbf{x}}) \cdot \widetilde{\mathbf{M}}_0^*(\mathbf{r}') \qquad (28)
$$

is the amplitude squared of the perturbation. Inserting Eq. (22) into Eq. (28), and then using Eq. (24) to take the ensemble average, we obtain the standard deviation

$$
\sigma_\kappa = [\langle\delta\kappa^2\rangle]^{1/2}, \qquad (29)
$$

$$
\simeq \sigma_e(\epsilon_2 - \epsilon_1)\Bigg\{ \sum_{l=1}^{N_d} \int_{-h/2}^{h/2}\int_{-h/2}^{h/2} dz\,dz' \int_0^{2\pi}\int_0^{2\pi} d\phi\,d\phi'\, e^{-a\Theta(\phi,\phi')/l_c}\widetilde{\mathbf{M}}_0[x_l + a\cos(\phi)+D, y_l + a\sin(\phi), z] \cdot \widetilde{\mathbf{M}}_0^*
$$

$$
\times [x_l + a\cos(\phi), y_l + a\sin(\phi), z]\widetilde{\mathbf{M}}_0^*[x_l + a\cos(\phi')+D, y_l + a\sin(\phi'), z'] \cdot \widetilde{\mathbf{M}}_0[x_l + a\cos(\phi'), y_l + a\sin(\phi'), z']
$$

$$
- \sum_{m=1}^{N_d} \int_{-h/2}^{h/2}\int_{-h/2}^{h/2} dz\,dz' \int_0^{2\pi}\int_0^{2\pi} d\phi\,d\phi'\, e^{-a\Theta(\phi,\phi')/l_c}\widetilde{\mathbf{M}}_0[x_m + a\cos(\phi)+D, y_m + a\sin(\phi), z] \cdot \widetilde{\mathbf{M}}_0^*
$$

$$
\times [x_m + a\cos(\phi), y_m + a\sin(\phi), z]\widetilde{\mathbf{M}}_0^*[x_m + a\cos(\phi')+D, y_m + a\sin(\phi'), z'] \cdot \widetilde{\mathbf{M}}_0
$$

$$
\times [x_m + a\cos(\phi'), y_m + a\sin(\phi'), z'] \Bigg\}^{1/2}, \qquad (30)
$$

where $N_d = 14$ is the number of air voids shifted to form the central cavity of the CCW (see Fig. 1), (x_l, y_l) are the coordinates of the air voids before they are shifted, and (x_m, y_m) are the coordinates after they are shifted.

In Fig. 5, we plot σ_{Ω_0} and σ_κ as functions of l_c. As both σ_{Ω_0} and σ_κ are proportional to σ_e, we set $\sigma_e = 3$ nm (a nominal value for high-quality structures) to simplify. We also adopt normalized units, $d/2\pi c$, for σ_{Ω_0} so it can be directly compared with σ_κ. Note that, from Eq. (4), to compare the relative effects of diagonal and off-diagonal disorders, we should compare $\sigma_{\Omega_0}/\Omega_0$ to σ_κ, where for our structure

$\Omega_0 \simeq 0.26(2\pi c)/d$. The key result is that first-order perturbation theory gives significant nonzero values for σ_{Ω_0}. This is because the mode field on the air-void boundaries, shown in Fig. 2, strongly varies as a function of ϕ producing nonzero values in the double integral over ϕ in Eq. (26). In planar and fiber waveguides, by contrast, it is clear that the first-order perturbation theory will give $\sigma_{\Omega_0} = 0$ irrespective of l_c (at least within the limits of our model) as the mode fields do not vary on the waveguide surfaces.

Examining Fig. 5 in more detail, we can see that σ_{Ω_0} and σ_κ have a similar dependence on l_c but that $\sigma_{\Omega_0}/\Omega_0$ is almost
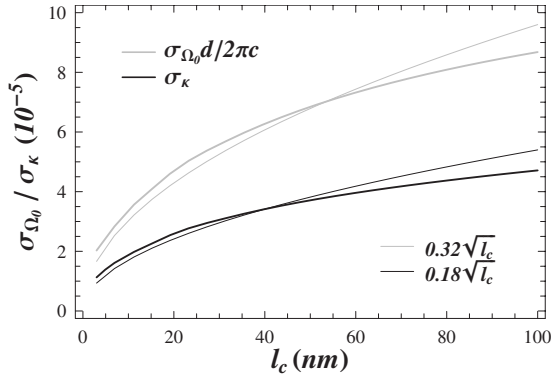
FIG. 5. Cavity-frequency and coupling-coefficient disorders. The normalized standard deviation of Ω_0, $\sigma_{\Omega_0}d/2\pi c$, and the standard deviation of κ and σ_κ are plotted for roughness with $\sigma_e = 3$ nm as a function of correlation length l_c.

an order of magnitude larger than σ_κ. This result is consistent with $\delta\omega_0$ in Eq. (17) and $\delta\kappa$ in Eq. (27) having similar functional forms. The main difference is that the mode fields are displaced in the calculation of κ, and thus $\sigma_\kappa < \sigma_{\Omega_0}/\Omega_0$. For roughness parameters of $\sigma_e = 3$ nm and $l_c = 40$ nm, $\sigma_{\Omega_0}/\Omega_0 = 2.4 \times 10^{-4}$ while $\sigma_\kappa = 3.4 \times 10^{-5}$. From this, we expect that the effect of off-diagonal disorder on the density of states (DOS) will be much less than the effect of diagonal disorder as we show explicitly in Sec. IV. An important property of both σ_{Ω_0} and σ_κ is that they are much more sensitive to σ_e than l_c. Their dependence on σ_e is clearly linear. The dependence on l_c, on the other hand, is approximately square root as shown in Fig. 5. For the wide range of l_c typically seen in experiment, $20 < l_c < 100$ nm, σ_{Ω_0} and σ_κ only vary by a factor of 2. We consider a lower bound for l_c to be $l_c > 3$ nm. However, even if fabrication could be improved to reduce l_c from $l_c = 20$ to 3 nm, σ_{Ω_0} and σ_κ would only be improved by a factor of 3.

The engineering task of minimizing disorder is to search for cavity modes that overlap least with the surfaces of the air voids as is clear from Eqs. (26) and (30). We have examined the cavity modes of most of the known high-Q PhCS cavities and σ_{Ω_0} is smallest for the Kuramochi cavity we have employed here. For the Noda cavity ($Q \approx 50\,000$),[12] $\sigma_{\Omega_0}/\Omega_0 \gtrsim 3.8 \times 10^{-4}$ when $\sigma_e = 3$ nm and $l_c = 40$ nm. Disorder is minimal in these two cavities because they are both essentially line-defect sections with cavity-mode fields strongly concentrated in large dielectric regions (see Fig. 2). By contrast, for the quadrupole mode of a point defect in a square lattice of air voids ($Q \approx 50\,000$),[37] $\sigma_{\Omega_0}/\Omega_0 \gtrsim 1.3 \times 10^{-3}$, while for the hexapole mode of a point defect in a hexagonal lattice ($Q \approx 10^6$),[38] $\sigma_{\Omega_0}/\Omega_0 \gtrsim 1.1 \times 10^{-3}$.

IV. DISORDER-INDUCED TRUNCATION OF THE DENSITY OF STATES

We now examine the effects of diagonal (variations in Ω_0) and off-diagonal disorders (variations in κ) on the DOS of a CCW. This problem has been addressed in detail for one-dimensional (1D) periodic structures in solid-state physics.[17]

Here, we apply the semianalytic methods of solid-state physics to disorder in periodic CCWs. We also use Monte-Carlo simulations to verify the semianalytic results and model disorder in finite CCWs.

We first examine diagonal disorder. It is reasonable to assume that the frequency shifts of individual cavities follow the Gaussian distribution

$$P_{\Omega_0}(\omega) = \frac{1}{\sqrt{2\pi}\sigma_{\Omega_0}} e^{-\omega^2/(2\sigma_{\Omega_0}^2)}. \quad (31)$$

This is because $\delta\omega_0$ is essentially a weighted summation of the finitely correlated random variable $R(\phi)$, and the central limit theorem for m-dependent variables[39] thus applies. In our finite CCW, we determine the ensemble average of the DOS with disorder, $\langle\rho(\omega)\rangle$, using a Monte-Carlo simulation. In each step, random shifts $[\delta\omega_0]_i$ with probability distribution $P_{\Omega_0}(\omega)$ are applied to the elements of Ω in Eq. (2). The eigenvalues of the perturbed equation are then calculated and the DOS is determined using Eq. (15). In the calculation, 2500 separate simulations are performed, and $\langle\rho(\omega)\rangle$ is obtained by taking the average of $\rho(\omega)$ at each frequency.

The average DOS can also be calculated semianalytically using the coherent-potential approximation (CPA).[17] Such an approach is essential for infinite CCWs where Monte-Carlo simulations cannot be employed. In the CPA, the average effect of disorder is captured by a frequency-dependent self-energy $\Sigma(\omega)$. The self-energy is the solution to[17]

$$\int d\omega' P_{\Omega_0}(\omega') \frac{\omega'}{1 - [\omega' - \Sigma(\omega)]\rho[\omega - \Sigma(\omega)]} = 0. \quad (32)$$

The simple form of $\rho(\omega)$ in a CCW makes numerically solving Eq. (32) straightforward. The average DOS is then given by $\langle\rho(\omega)\rangle = \rho[\omega - \Sigma(\omega)]$.

In Fig. 6, we plot the DOS with diagonal disorder for surface roughness parameters of $\sigma_e = 3$ nm and $l_c = 3$ and 40 nm. In the Monte-Carlo simulations we take a finite CCW with $N = 301$. As can be seen, the DOS in the infinite CCW calculated using the CPA is an accurate and smooth representation of the DOS in the finite CCW calculated using the Monte-Carlo method. The oscillations in the finite structure near band center are simply the Fabry-Perot oscillations due to the finite size just as in Fig. 3. The disorder has little effect on the midband DOS or the bandwidth of the CCW. The main effect is to broaden the band-edge peak in the DOS. For a state-of-the-art correlation length of $l_c = 40$ nm, the broadening dramatically reduces the peak LDOS by roughly a factor of 2.5. We also employ $l_c = 3$ nm as an approximate theoretical lower limit, below which the lattice constant of the dielectric material prevents further refinement. At this level, broadening is smaller but still significant.

To provide further insight on the DOS broadening caused by diagonal disorder, we determine the dependence of the broadening on the key parameters. First, we note that $\langle\rho(\omega)\rangle$ can be approximated by $\rho_{dis}(\omega) = \rho(\omega)$ given by Eq. (16) but with γ_0 replaced with an effective linewidth γ_{eff}, which includes the disorder-induced broadening. Furthermore, we know from recent analysis[19] that CCW performance decreases as disorder increases relative to the CCW bandwidth
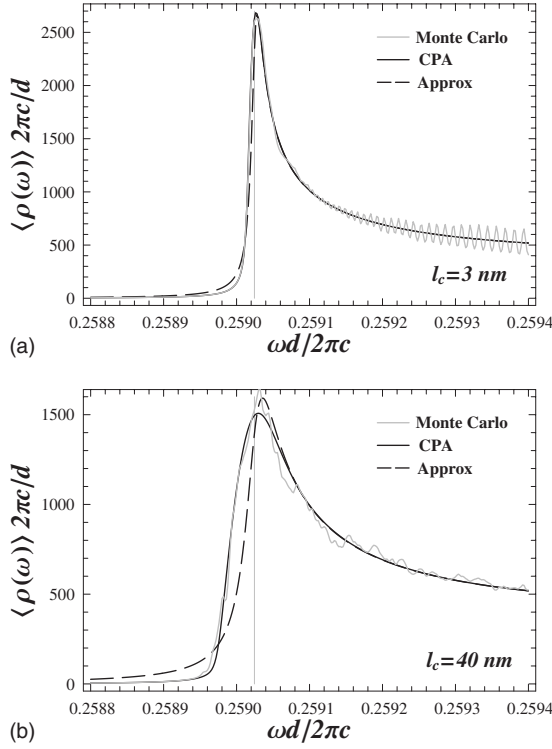
FIG. 6. DOS in a CCW with diagonal disorder. The disorder is for surface roughness with σ_e=3 nm, where (a) l_c=3 and (b) 40 nm. The average DOS is calculated numerically using the Monte-Carlo method and semianalytically using the CPA. The approximate DOS obtained using γ_{eff} is also shown.

$2 \Omega_0 \kappa$. The relation between band-edge broadening and CCW bandwidth can be quantified by recognizing that the DOS with diagonal disorder is invariant when the normalized frequency, $\omega' = \omega/v$, is employed, where $v = \sigma_{\Omega_0}^{4/3}/(2 \Omega_0 \kappa)^{1/3}$ is the scaling parameter.[18] Assuming a linear relation between γ_{eff} and v, we find from regression analysis that

$$\gamma_{eff} \simeq \frac{1}{\sqrt{2}} \frac{\sigma_{\Omega_0}^{4/3}}{(2 \Omega_0 \kappa)^{1/3}} + \gamma_0. \qquad (33)$$

In Fig. 6, we plot $\rho_{dis}(\omega)$ using γ_{eff} (labeled as "approx") showing that it is a good approximation to $\langle \rho(\omega) \rangle$. For l_c =3 nm, γ_{eff}=6.8×10⁻⁶ with a corresponding effective Q of Q_{eff}=19 000. For l_c=40 nm, γ_{eff}=1.9×10⁻⁵ with a corresponding effective Q of Q_{eff}=6800. Recalling that Q_0 =38 600, *extrinsic loss due to diagonal disorder is thus much greater than intrinsic loss*. Although this simple model of the DOS accurately captures the width and height of the band-edge DOS, it does not accurately capture the change in the shape of the DOS at the band edge; in contrast to our simplified model, the calculated diagonal disorder produces a small increase in the CCW bandwidth and steepens the DOS at the band edge.

We next examine the effects of off-diagonal disorder on the DOS. In Fig. 7, we plot the DOS with off-diagonal disorder for surface roughness parameters of σ_e=3 nm and l_c =40 nm. This is done in the finite CCW using a Monte-
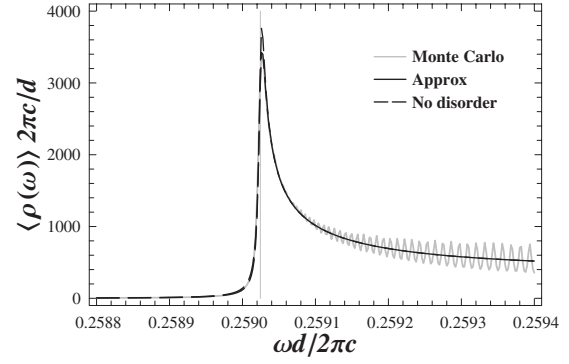

FIG. 7. DOS in a CCW with off-diagonal disorder. The disorder is for surface roughness with σ_e=3 nm and l_c=40 nm. The average DOS is calculated using the Monte-Carlo method. The approximate DOS is calculated using γ_{eff}=4.0×10⁻⁶. The DOS with no disorder is shown for reference.

Carlo simulation. The CPA can also be used[17] but requires more work than the diagonal case. We approximately quantify the DOS broadening by choosing γ_{eff} to fit $\rho_{dis}(\omega)$ to $\langle \rho(\omega) \rangle$. The result is γ_{eff}=4.0×10⁻⁶, which is only marginally larger than the unperturbed value of γ_0=3.37×10⁻⁶. The effect of off-diagonal disorder is thus small compared to diagonal disorder. Note also that off-diagonal disorder does not significantly change the shape of the DOS. It is clear that diagonal disorder will dominate off-diagonal disorder even when $\sigma_{\Omega_0}/\Omega_0 \sim \sigma_\kappa$ as the former is a first-order perturbation to the CCW mode frequencies, while the latter is a second-order perturbation.

We close this section by noting that the results for both the Monte-Carlo and CPA simulations are ensemble averages over many structures. That is, the calculated DOS is the average DOS that we would obtain if the DOS of many structures were measured. In any given structure and at any given point in that structure, the DOS (LDOS) could be considerably different than that presented. What our results provide is what we would expect to see on average in such structures. This motivates the need to perform experimental measurements over many samples and present the average. Only then can we have confidence in what is going on for a specific design or nominally fabricated structure. This point, although obvious, is rarely pointed out or investigated by experimental groups as it is tempting to measure and report the "best measured" samples.

V. IMPLICATIONS FOR SLOW LIGHT AND BAND-EDGE INTERACTIONS

Coupled-cavity waveguides can potentially support very low group velocities, either across their bandwidth when κ is small or at their band edges. The effect of disorder on group velocities can be determined approximately using the DOS.[20] As $\rho(\omega)d\omega = \bar{\rho}(k)dk$, where $\bar{\rho}(k)$ is the DOS in k space, the group velocity is given by the DOS according to

$$v_g \equiv \frac{d\omega}{dk},$$

$$= \frac{\bar{\rho}(k)}{\rho(\omega)},$$

$$= \frac{D}{\pi\rho(\omega)}. \tag{34}$$

The group velocity is thus simply inversely proportional to the DOS.

We first use the DOS in Fig. 3 to examine the effect of intrinsic loss on slow light in CCWs. In the absence of surface roughness, the minimum propagation speed of light in the structure is limited by the linewidth of the individual cavities. In this ideal (intrinsic) case, the minimum group velocity occurs at the band edge and from Eqs. (16) and (34) it is found to be given approximately by

$$v_g^{\min} = D\sqrt{4\gamma_0\,\Omega_0\kappa}. \tag{35}$$

For our CCW, this results in a minimum (intrinsic) band-edge group velocity of $v_g = c/330$.

We now use the ensemble-averaged DOS in Fig. 6 to examine the effect of diagonal disorder on slow light. In this case, the group velocity that we obtained is an effective ensemble-averaged group velocity. For surface roughness parameters of $\sigma_e = 3$ nm and $l_c = 3$ nm, using Eq. (34) the band-edge group velocity is found to be $v_g = c/220$. Thus, even at the theoretical lower limit for surface roughness, the velocity of slow light in CCWs in PhCSs remains high. For more realistic surface roughness parameters of $\sigma_e = 3$ nm and $l_c = 40$ nm, the band-edge group velocity is found to be $v_g = c/120$. Despite employing a different waveguiding mechanism, these values appear to be consistent with the experimental values of $v_g \approx c/100$ (Ref. [40]) and $c/300$ (Ref. [41]) that have been observed in silicon line-defect waveguides in PhCSs at wavelengths of $\lambda \sim 1500$ nm, although, as is now well accepted, these modes are very lossy and are dominated by back-scatter losses.

An approximate expression for minimum group velocity can be obtained by simply substituting γ_{eff} with γ_0 in Eq. (35) to give

$$v_g^{\mathrm{eff}} = D\sqrt{2\gamma_{\mathrm{eff}}B}, \tag{36}$$

where $B \equiv 2\,\Omega_0\kappa$ is the width of the band. This expression gives good agreement with the calculated results for the two different values of l_c discussed above. The above expression should be approximately correct for other waveguides such as a line-defect waveguide as long as γ_{eff} can be determined; However, the precise expression for γ_{eff} will not be given by Eq. (33). In cases where $\gamma_{\mathrm{eff}} \gg \gamma_0$, we can use Eq. (33) to obtain the following simple expression for the minimum group velocity:

$$v_g^{\mathrm{eff}} = \frac{D(\Omega_0\kappa)^{1/3}}{2^{7/12}}\sigma_{\Omega_0}^{2/3}. \tag{37}$$

Thus, from Eq. (26) we see that when surface roughness dominates, the minimum group velocity scales approximately as $v_g^{\mathrm{eff}} \propto \Omega_0\kappa^{1/3}\sigma_e^{2/3}$.

Our numerical results for the DOS (and hence the group velocity) are calculated for a finite CCW with $N = 301$. We have chosen this number because the DOS near band edge for this finite structure is essentially identical to that of an infinite structure. We could choose a somewhat smaller N, but for much smaller values of N or away from band edge, the results from the DOS of a finite structure would not be accurate. Furthermore, when N is small, the concept of group velocity becomes unclear and certainly cannot be calculated simply using the DOS.

We now briefly consider the group velocity at band center. From Figs. 3 and 6, we see that the DOS for the structure at band center is almost unaffected by surface roughness. Thus, the group velocity at band center is essentially the same, both with and without surface roughness. Again using Eqs. (16) and (34) the band-center group velocity is found to be given approximately by

$$v_g^{\max} = D\,\Omega_0\kappa. \tag{38}$$

For the structure considered, this gives a midband group velocity of $v_g \simeq c/47$. Of course, if the coupling becomes weaker and/or the spacing between cavities increases, this maximum velocity will decrease. However, $v_g^{\max}$ will remain independent of the degree of surface roughening and will be given by Eq. (38) as long as the width of the band is much larger than the effective broadening; that is, as long as $\Omega_0\kappa/\gamma_{\mathrm{eff}} \gg 1$. For our CROW with $\sigma_e = 3$ nm and $l_c = 3$ nm, $\Omega_0\kappa/\gamma_{\mathrm{eff}} \simeq 170$.

The sharp peak in the DOS at the band edge of CCWs could potentially produce strong interactions with embedded quantum dots (QDs). Much of the early work on band-edge quantum optics was performed using the isotropic band-edge model for the DOS with $1/\sqrt{\omega - \omega_l}$. The interesting feature of a CCW is that the isotropic model applies directly. Equation (16) is essentially the isotropic model but with both the lower and upper band edges. Furthermore, loss is included in a very simple way via the complex $\tilde{\omega}_l$ and $\tilde{\omega}_u$. This makes it possible to parametrize the effect of loss on band-edge interactions.

The strong coupling between an atom or QD and a single cavity is a well-known problem.[42] The coupling coefficient between a QD and a cavity mode is given by

$$g = \mu\sqrt{\frac{\omega_a}{2\hbar\epsilon_0}}|\tilde{\mathbf{M}}_0(\mathbf{r}_{\mathrm{QD}})\cdot\hat{\mathbf{d}}|, \tag{39}$$

where ω_a is the QD transition frequency and $\mathbf{r}_{\mathrm{QD}}$ is the QD position. If the linewidth of the cavity resonance, γ_0, is larger than the nonradiative linewidth of the QD, γ_a, then the condition for strong coupling is[43]

$$2g > \gamma_0. \tag{40}$$

The condition is that the Rabi frequency, $\Omega_R = 2g$, of the coupling between the QD and the cavity mode is greater than the rate of decay out of the cavity mode.

At the band edge of a CCW, the Rabi frequency is[8,44]

$$\Omega_R = g^{4/3}/(2\omega_a\kappa)^{1/3}. \tag{41}$$

When disorder is included, the effective linewidth of the band edge is given by γ_e in Eq. (33). The condition for strong coupling at the band edge thus becomes

$$\Omega_R > \gamma_{\text{eff}}. \tag{42}$$

Employing Eqs. (33) and (41) and assuming $\gamma_0 \ll \gamma_{\text{eff}}$, the condition simplifies to

$$g > \frac{1}{2^{3/8}}\sigma_{\Omega_0}. \tag{43}$$

Interestingly, this condition is independent of the bandwidth of the CCW and is simply determined by the QD coupling coefficient and the level of diagonal disorder.

For a typical self-assembled semiconductor QD with a dipole moment of $\mu = 30$ D, which is aligned optimally with the cavity mode (in polarization and spatial position), the QD cavity-mode coupling coefficient in our cavity is $g = 9$ GHz. Equation (43) consequently implies that σ_{Ω_0} must be below the critical value of $\sigma_{\Omega_0}^c = 11$ GHz in order to achieve strong coupling. For roughness parameters of $\sigma_e = 3$ nm and $l_c = 40$ nm, however, $\sigma_{\Omega_0} = 45$ GHz, which is a factor of 4 above the critical value. For $l_c = 3$ nm, the disorder improves to $\sigma_{\Omega_0} = 14$ GHz, which is still a factor of 5/4 above the critical value. We note that the critical value is only indicated when the QD decay dynamics becomes nonexponential (of course, neglecting the nonexponential behavior of nonradiative decay at higher temperatures usually mediated by electron-phonon or nonlinear interactions[45]). To see the effect of the formation of a quasistable state at a band edge,[44] $\sigma_{\Omega_0} \lesssim \sigma_{\Omega_0}^c/5$.[8] For state-of-the-art fabrication, disorder due to surface roughness is thus still well over an order of magnitude greater than that required to see the interesting quantum optical effect predicted at a photonic band edge.[8,44]

Although the disorder appears to destroy the possibility of strong-coupling dynamics at the band edge, at least for nominal QD dipole moments, the CCW with a QD could still be used as a fast directional single-photon source due to its large Purcell factor, F_p, at the band edge. To clarify this point, we compare the peak Purcell factor F_p^{CCW} of the CCW with disorder to the Purcell factor F_p^{cav} of one of the cavities in the CCW. From our previous results, it is easily seen that in the nearest-neighbor tight-binding (NNTB) approximation,

$$F_p^{\text{CCW}} = \sqrt{\frac{Q_{\text{eff}}}{8\kappa}}QF_p^{\text{cav}}. \tag{44}$$

Using the values for our CCW, we see that in the absence of disorder, $F_p^{\text{CCW}} \simeq 0.035F_p^{\text{cav}}$, while with $\sigma_e = 3$ nm and $l_c = 40$ nm, F_p^{CCW} is only reduced by a factor of 2.3. Given that the peak Purcell factor for the single cavity is[6,32] $F_p^{\text{cav}} = 6\pi c^3 Q/(V_{\text{eff}}\Omega_0^3\epsilon^{3/2}) \approx 1680$, we see that reasonably large Purcell factors are possible for this structure ($F_p^{\text{CCW}} \approx 26$). As for the group velocity, this result is consistent with experimental results in line-defect waveguides. Recent observations by Lund-Hansen et al.[46] clearly see the reduction of the expected Purcell factor near band edge.

VI. CONCLUSIONS

In conclusion, we have introduced two important results regarding the effects of unavoidable fabrication disorder due to the surface roughness of PhCS couple-cavity waveguides. First, because cavity-mode fields vary strongly around the circumference of the air voids, any correlation in the roughness along the circumference will produce significant disorder in the form of variations in the individual cavity-mode frequencies. Our results suggest that the influence of disorder on the band-edge optical properties may be minimized by using cavity-mode fields that (1) weakly overlap with the air-void boundaries or (2) vary weakly on the circumference of the air-void boundaries. Given that the pool of high-Q PhCS cavity modes is small and we have calculated the disorder in most without improving the results, it would appear that the room for optimization is small.

The second key result is that surface roughness dramatically reduces the capacity of CCWs in PhCSs to produce slow-light and strong band-edge interactions. This is particularly easy to see in a CCW as the band-edge broadening of the DOS can be simply parametrized in terms of the disorder. In a state-of-the-art PhCS, the smallest group velocity achievable is around $c/120$, while the disorder is an order of magnitude greater than that required to achieve strong band-edge coupling with a QD. Even if surface roughness could be reduced to atomic scales, the improvements would not seem to be sufficient to allow strong band-edge coupling in the structure investigated. However, even with disorder, CCWs may still be good candidates for single-photon sources due to the reasonable Purcell factor and directional emission, although with a caveat that the propagation mode is then very lossy. In addition, while we find that the effect of disorder on the band-edge DOS is significant, at band center the DOS is largely insensitive–though either region will inevitably result in enhanced disorder-induced propagation loss if used in a slow-light regime.[25,26]

Last, but not least, our results motivate the essential need for experimentalists to present an ensemble of measurements on nominally identical samples, which is critically important for future applications. Indeed, this latter point is generally true for all PhCS structures.

[1] A. Yariv, Y. Xu, R. K. Lee, and A. Scherer, Opt. Lett. **24**, 711 (1999).

[2] N. Stefanou and A. Modinos, Phys. Rev. B **57**, 12127 (1998).

[3] S. Mookherjea and A. Yariv, Phys. Rev. E **64**, 066602 (2001).

[4] J. Poon, J. Scheuer, Y. Xu, and A. Yariv, J. Opt. Soc. Am. B **21**, 1665 (2004).

[5] S. Mookherjea and A. Yariv, Phys. Rev. E **65**, 026607 (2002).

[6] V. S. C. Manga Rao and S. Hughes, Phys. Rev. B **75**, 205437 (2007).

[7] G. Lecamp, P. Lalanne, and J. P. Hugonin, Phys. Rev. Lett. **99**, 023902 (2007).

[8] D. P. Fussell and M. M. Dignam, Phys. Rev. A **76**, 053801 (2007).

[9] S. Olivier, C. Smith, M. Rattier, H. Benisty, C. Weisbuch, T. Krauss, R. Houdre, and U. Oesterle, Opt. Lett. **26**, 1019 (2001).

[10] T. J. Karle, D. H. Brown, R. Wilson, M. Steer, and T. F. Krauss, IEEE J. Quantum Electron. **8**, 909 (2002).

[11] P. Sanchis, J. Martí, W. Bogaerts, P. Dummon, D. Van Thourhout, and R. Baets, IEEE Photonics Technol. Lett. **17**, 1199 (2005).

[12] Y. Akahane, T. Asano, B.-S. Song, and S. Noda, Nature (London) **425**, 944 (2003).

[13] E. Kuramochi, M. Notomi, S. Mitsugi, A. Shinya, and T. Tanabe, Appl. Phys. Lett. **88**, 041112 (2006).

[14] D. O'Brien, M. Settle, T. Karle, A. Michaeli, M. Salib, and T. Krauss, Opt. Express **15**, 1228 (2007).

[15] M. L. Povinelli and S. Fan, Appl. Phys. Lett. **89**, 191114 (2006).

[16] D. P. Fussell and M. M. Dignam, Appl. Phys. Lett. **90**, 183121 (2007).

[17] E. N. Economou, *Green's Functions in Quantum Physics* (Springer-Verlag, New York, 1990).

[18] E. N. Economou, C. M. Soukoulis, M. H. Cohen, and A. D. Zdetsis, Phys. Rev. B **31**, 6172 (1985).

[19] e.g., see B. Z. Steinberg, A. Boag, and R. Lisitsin, J. Opt. Soc. Am. A **20**, 138 (2003).

[20] S. Mookherjea and A. Oh, Opt. Lett. **32**, 289 (2007); S. Mookherjea and A. Oh, Conference on Lasers and Electro-Optics, 2007 (unpublished), Paper No. CthG3.

[21] M. Bayindir, B. Temelkuran, and E. Ozbay, Phys. Rev. Lett. **84**, 2140 (2000).

[22] J. K. S. Poon, L. Zhu, G. DeRose, and A. Yariv, Opt. Lett. **31**, 456 (2006).

[23] M. Skorobogatiy, G. Begin, and A. Talneau, Opt. Express **13**, 2487 (2005).

[24] F. P. Payne and J. P. Lacey, Opt. Quantum Electron. **26**, 977 (1994).

[25] S. Hughes, L. Ramunno, J. F. Young, and J. E. Sipe, Phys. Rev. Lett. **94**, 033903 (2005).

[26] E. Kuramochi, M. Notomi, S. Hughes, A. Shinya, T. Watanabe, and L. Ramunno, Phys. Rev. B **72**, 161318(R) (2005).

[27] T. Kamalakis and T. Sphicopoulos, IEEE J. Quantum Electron. **41**, 1419 (2005).

[28] W. C. Chew, *Waves and Fields in Inhomogeneous Media* (IEEE, New York, 1995).

[29] R. J. Glauber and M. Lewenstein, Phys. Rev. A **43**, 467 (1991).

[30] M. Wubs, L. G. Suttorp, and A. Lagendijk, Phys. Rev. A **70**, 053823 (2004).

[31] D. P. Fussell, M. M. Dignam, M. J. Steel, C. M. de Sterke, and R. C. McPhedran, Phys. Rev. A **74**, 043806 (2006).

[32] See, e.g., J. Vučković, M. Pelton, A. Scherer, and Y. Yamamoto, Phys. Rev. A **66**, 023808 (2002).

[33] S. Hughes, Opt. Lett. **29**, 2659 (2004).

[34] S. G. Johnson, M. L. Povinelli, M. Soljacic, A. Karalis, S. Jacobs, and J. D. Joannopoulos, Appl. Phys. B: Lasers Opt. **81**, 283 (2005).

[35] L. C. Andreani and D. Gerace, Phys. Status Solidi B **244**, 3528 (2007).

[36] L. Ramunno and S. Hughes (unpublished).

[37] H.-Y. Ryu, S.-H. Kim, H.-G. Park, J.-K. Hwang, Y.-H. Lee, and J.-S. Kim, Appl. Phys. Lett. **80**, 3883 (2002).

[38] H.-Y. Ryu, M. Notomi, and Y.-H. Lee, Appl. Phys. Lett. **83**, 4294 (2003).

[39] H. J. Godwin and S. K. Zaremba, Ann. Math. Stat. **32**, 677 (1961).

[40] M. Notomi, K. Yamada, A. Shinya, J. Takahashi, C. Takahashi, and I. Yokohama, Phys. Rev. Lett. **87**, 253902 (2001).

[41] Y. A. Vlasov, M. O'Boyle, H. F. Hamann, and S. J. McNab, Nature (London) **438**, 65 (2005).

[42] H. J. Carmichael, *Statistical Methods in Quantum Optics 2* (Springer, New York, 2008).

[43] L. C. Andreani, G. Panzarini, and J.-M. Gerard, Phys. Rev. B **60**, 13276 (1999).

[44] S. John and T. Quang, Phys. Rev. A **50**, 1764 (1994).

[45] J. Förstner, C. Weber, J. Danckwerts, and A. Knorr, Phys. Rev. Lett. **91**, 127401 (2003).

[46] T. Lund-Hansen, S. Stobbe, B. Julsgaard, H. Thyrrestrup, T. Sünner, M. Kamp, A. Forchel, and P. Lodahl, Phys. Rev. Lett. **101**, 113903 (2008).